Molecular Cell, Vol. 9, 423–432, February, 2002, Copyright ©2002 by Cell Press

Three-Dimensional Structure of the Apoptosome: Implications for Assembly, Procaspase-9 Binding, and Activation

Devrim Acehan,[1] Xuejun Jiang,[2] David Gene Morgan,[1,3] John E. Heuser,[4] Xiaodong Wang,[2] and Christopher W. Akey[1,5]

[1]Department of Physiology and Biophysics
Boston University School of Medicine
700 Albany Street
Boston, Massachusetts 02118

[2]Howard Hughes Medical Institute and
Department of Biochemistry
University of Texas
Southwestern Medical Center at Dallas
Dallas, Texas 75235

[3]Howard Hughes Medical Institute and
Department of Cell Biology
Harvard Medical School
240 Longwood Avenue
Boston, Massachusetts 02115

[4]Department of Cell Biology
Washington University School of Medicine
660 South Euclid Avenue
St. Louis, Missouri 63110

Summary

The apoptosome is an Apaf-1 cytochrome c complex that activates procaspase-9. The three-dimensional structure of the apoptosome has been determined at 27 Å resolution, to reveal a wheel-like particle with 7-fold symmetry. Molecular modeling was used to identify the caspase recruitment and WD40 domains within the apoptosome and to infer likely positions of the CED4 homology motif and cytochrome c. This analysis suggests a plausible role for cytochrome c in apoptosome assembly. In a subsequent structure, a noncleavable mutant of procaspase-9 was localized to the central region of the apoptosome. This complex promotes the efficient activation of procaspase-3. Therefore, the cleavage of procaspase-9 is not required to form an active cell death complex.

Introduction

Apoptosis is the dominant form of programmed cell death during embryonic development and normal tissue turnover. This death process may also occur as a cellular response to stress or pathogens (reviewed in Aravind et al., 1999). In addition, apoptosis is upregulated in diseases such as AIDS, neurodegenerative disorders, and ischemic stroke (Thompson, 1995), while it is downregulated in certain cancers (Song and Steller, 1999; Salvesen and Dixit, 1997). In apoptosis, death signals are transduced by biochemical pathways to activate caspases, a group of proteases that utilize cysteine at their active sites to cleave specific proteins at aspartate residues (Song and Steller, 1999). The proteolysis of these critical proteins then initiates cellular events that include chromatin degradation into nucleosomes and organelle destruction (Budihardjo et al., 1999; Salvesen and Dixit, 1997). These steps prepare apoptotic cells for phagocytosis and result in the efficient recycling of biochemical resources (Desagher and Martinou, 2000).

In many cases, apoptotic signals are transmitted to mitochondria, which act as integrators of cell death because both effector and regulatory molecules converge at this organelle. Apoptosis mediated by mitochondria requires the release of cytochrome c into the cytosol (Liu et al., 1996; Goldstein et al., 2000) through a process that may involve the formation of specific pores or rupture of the outer membrane (reviewed in Desagher and Martinou, 2000; Budihardjo et al., 1999). Cytochrome c binds to Apaf-1 and in the presence of dATP/ATP promotes assembly of the apoptosome. This large protein complex then binds and activates procaspase-9 (Srinivasula et al., 1998; Zou et al., 1997, 1999; Li et al., 1997; Hu et al., 1999). A nonhydrolyzable ATP analog (ADP-CP) also promotes apoptosome formation. This suggests that assembly may be initiated by nucleotide binding rather than hydrolysis (Jiang and Wang, 2000). Procaspase-9 contains a caspase recruitment domain (CARD) that is used to mediate specific interactions with the Apaf-1 CARD, which becomes exposed on the apoptosome during assembly (Srinivasula et al., 1998; Zou et al., 1999). The precise size, number of subunits, and structure of the apoptosome are not known. In addition, the mechanism of procaspase-9 activation on the apoptosome has not been determined (see Budihardjo et al., 1999). After cleavage, mature caspase-9 remains bound to the apoptosome where it is able to activate executioner caspases such as caspase-3 and -7 (Rodriguez and Lazebnik, 1999).

Apaf-1 is a multidomain protein comprised of an N-terminal CARD, a central CED4 homology motif that binds dATP/ATP, and 12 or 13 WD40 repeats in the C-terminal region (Zou et al., 1997, 1999; Li et al., 1997; Hu et al., 1998). The CED4 protein from *C. elegans* does not contain WD40 repeats, but oligomer formation is required for apoptotic activity (Yang et al., 1998). A truncated Apaf-1, in which the WD40 repeats have been removed, no longer binds cytochrome c and is constitutively active (Srinivasula et al., 1998; Hu et al., 1999). Hence, the WD40 repeats may function as intramolecular inhibitors of apoptosome assembly. This autoinhibition is overridden by cytochrome c which promotes assembly in the presence of dATP/ATP (Srinivasula et al., 1998; Hu et al., 1999; Jiang and Wang, 2000). The importance of cytochrome c is highlighted in cell lines that lack this electron carrier. When grown under conditions that mitigate the loss of cytochrome c, these cells failed to form the apoptosome and failed to activate procaspase-9 in response to proapoptotic stimuli (Li et al., 2000).

In this work, the three-dimensional (3D) structure of the apoptosome has been determined at 27 Å resolution. We also determined the structure of apoptosomes containing a noncleavable mutant of procaspase-9 and located the zymogen binding site. These data suggest a model for the role of cytochrome c in promoting assem-

[5]Correspondence: akey@med-biophm.bu.edu

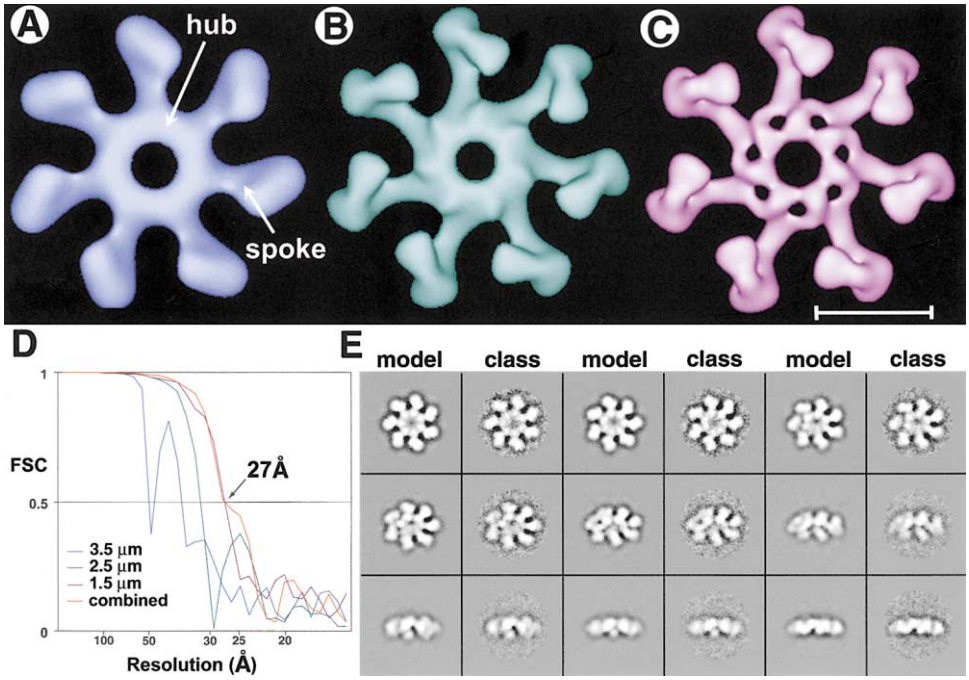

Figure 1. Structure Determination

(A) The apoptosome is a wheel-like particle at ~50 Å resolution with seven spokes and a central hub.

(B) The distal region of the spoke has a pronounced Y shape at ~35 Å resolution.

(C) At ~27 Å resolution, the connectivity of the central hub is revealed due in part to the diminished contrast of the low spatial frequency components. The maps in (A)–(C) are not CTF corrected. The scale bar is 100 Å.

(D) Fourier shell correlation curves were used to estimate the resolution in each of the 3D datasets with a conservative cutoff of 0.5.

(E) Nine projections are shown from the final 3D model. These views are paired with the corresponding class averages.

bly of the apoptosome and provide insights into the mechanism of procaspase-9 activation.

Results

Structure of the Apaf-1 Cytochrome C Complex

The low abundance of human Apaf-1 led us to overexpress the His-tagged protein in insect cells. For these studies, Apaf-1 with 13 WD40 repeats (1248 residues) was used because it is more active than the isoform with 12 repeats (Srinivasula et al., 1998; Zou et al., 1999; Hu et al., 1999). Although the purified monomer is labile, we obtained efficient assembly of Apaf-1, cytochrome c, and dATP to form a functional apoptosome (see later discussion and Figures 5A and 5B). Samples were prepared for electron cryomicroscopy by plunge freezing, and micrographs were recorded for image processing. Our initial survey suggested that apoptosomes have 7-fold rotational symmetry under the conditions used for in vitro assembly. Particles with 6-fold symmetry were also observed, but they represent a small percentage of the total population (<1%). Thus, we have used apoptosomes with 7-fold symmetry to determine a low resolution 3D map.

Apoptosomes have an unusual aspect ratio (~270 × 70 Å) that produces low contrast in many particle views. Therefore, we collected images in three defocus groups and first processed the most strongly defocused data to take advantage of the better signal-to-noise ratio. The EMAN package (Ludtke et al., 1999) was used to calculate a low resolution 3D model (Figure 1A). This reference was used to calculate two intermediate structures with stepwise increases in resolution (Figures 1B and 1C). A total of ~3400 particles was then corrected for the contrast transfer function and combined to give a final map with a resolution of ~27 Å (Figure 1D). Projection pairs from the final 3D model and the corresponding class averages are shown in Figure 1E. The 7-fold symmetry of the model was not imposed upon the classes, which reflect averages of individual particles aligned in a similar orientation.

The apoptosome is a wheel-like particle with seven spokes that radiate from a central hub (Figures 1A–1C, 1E, and 2A), and has a calculated mass of ~1 MDa. In Figure 2, the apoptosome is rotated about a horizontal axis (see arrow) to reveal different views of the complex. The concave hub and the bent spokes combine to give the apoptosome a puckered shape (Figure 2D). The hub domain is connected to the Y domain by a bent arm. The bend in the arm occurs at an "elbow" located proximal to the hub (see asterisk in Figure 2D). Each Y domain is comprised of two lobes with density between them (see bridge, Figure 2B). By raising the threshold, we were able to delineate a possible path for the Apaf-1 monomer within the apoptosome (see black line in Figure 2B). Thus, each Apaf-1 molecule contributes a hub domain, an arm, and a Y domain to the apoptosome (Figures 2A and 2B).

Rotary shadowing experiments were carried out with the apoptosome and Apaf-1 to confirm our model (Figure 3). We found that apoptosomes were bound preferentially to the mica to give bottom views that were better

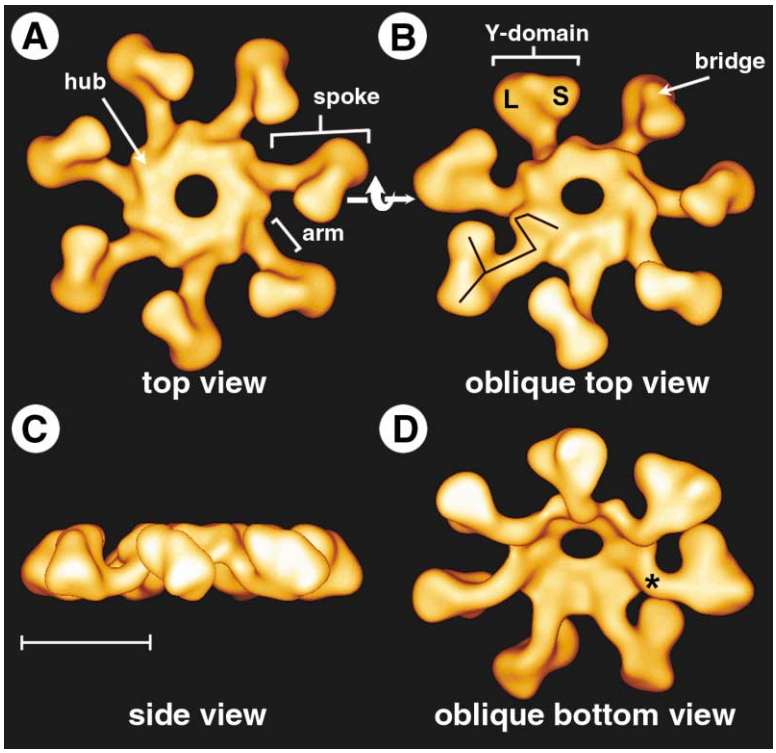

Figure 2. Three-Dimensional Structure of the Apoptosome

The final 3D structure of the apoptosome from all CTF-corrected particles is shown as a series of surface views that are related by rotations about the horizontal arrow.

(A) The apoptosome is shown in a top view along the 7-fold symmetry axis. Features of interest are labeled, including the central hub, the spoke, and the arm.

(B) Details of the spoke are evident in an oblique top view. They include the Y domain with two lobes that are marked large (L) and small (S). A bridge is located between the two lobes. By varying the threshold, we delineated the most likely path for an Apaf-1 monomer by tracing the regions with strongest connectivity within the hub (see Y-shaped black line).

(C) A side view of the apoptosome reveals the unusual axial ratio of this particle. The scale bar is 100 Å.

(D) An oblique bottom view shows the puckered shape of the particle. The arms are bent at an elbow (see asterisk) located proximal to the hub.

preserved than top views (Figure 3A, compare panels 1–3 with 4). These images confirmed the 7-fold symmetry of the particles and also showed a two-lobed architecture for each spoke, consistent with our 3D model. However, we could not determine the handedness of the apoptosome due in part to flattening effects. Experiments with Apaf-1 monomers revealed two principal conformations. These included Y-shaped molecules with a small globular domain located at the base of the tail (Figure 3B, see panels 2, 3, 4, 7, and 8) and molecules with a compact shape (Figure 3B, e.g., panels 5, 11, and 12). When combined with our 3D structure, the data suggest that Apaf-1 adopts a Y-like conformation within the apoptosome. The possible significance of the compact monomers will be discussed later.

Domain Architecture of Apaf-1 and Interactions with Cytochrome C

The primary sequence of human Apaf-1 is readily divided into three major regions, including an N-terminal CARD, a central CED4 homology motif, and a large C-terminal tract containing 12 or 13 WD40 repeats (Zou et al., 1999; Figure 7A). To date, there are no high resolution structures available for the Apaf-1 CED4 homology and WD40 domains. However, crystallographic structures for the Apaf-1 CARD, cytochrome c, and a number of WD40 and Kelch repeat domains are available. Hence, we tried to locate Apaf-1 sequence motifs and cytochrome c within the framework of the apoptosome map. In this approach, high resolution domain structures were placed within the 3D map using the graphics program "O" (Jones et al., 1991), to identify regions with a similar size and shape.

We started with the 13 WD40 repeats because they are expected to form β propellers (see Smith et al., 1999). In these domains, four β strands pack together to form a blade-like feature and multiple blades are then arranged with a cyclic symmetry that corresponds to the number of WD40 or Kelch repeats. Inspection of the apoptosome suggests that each lobe within the Y domain is roughly the right size and shape to be a β propeller. In addition, no other region of the apoptosome is big enough to accommodate the β propellers. We next placed β propellers with five, six, seven, and eight blades into the two lobes of the Y. Although the thickness of a β propeller is similar within the WD40 and Kelch families, its diameter increases significantly with the addition of each blade. We found that one lobe of the Y is markedly larger (Figure 2B, marked L), and this region can accommodate a seven-blade β propeller (Figures 4A and 4C), while the smaller lobe (Figure 2B, marked S) is better fit with a six-blade β propeller (Figures 4B and 4C). The ~150 residues between the CED4 homology motif and the WD40 repeats, along with a linker of ~50 residues between WD40 repeats seven and eight, may form connections between the arm and the two β propellers. At this stage, the limited resolution of the map and the lack of high resolution structures for the Apaf-1 β propellers prevent us from attaining a precise molecular docking. However, the fit of the seven- and six-blade β propellers suggests that they face outwards away from the center of the Y domain with an angle of ~90° between them (Figure 4C).

Biochemical evidence suggests that cytochrome c may trigger apoptosome assembly by interacting with the WD40 repeats (Srinivasula et al., 1998; Hu et al., 1999). We noticed that the bridge region between the lobes of the Y (Figure 2B) is left empty after placing the

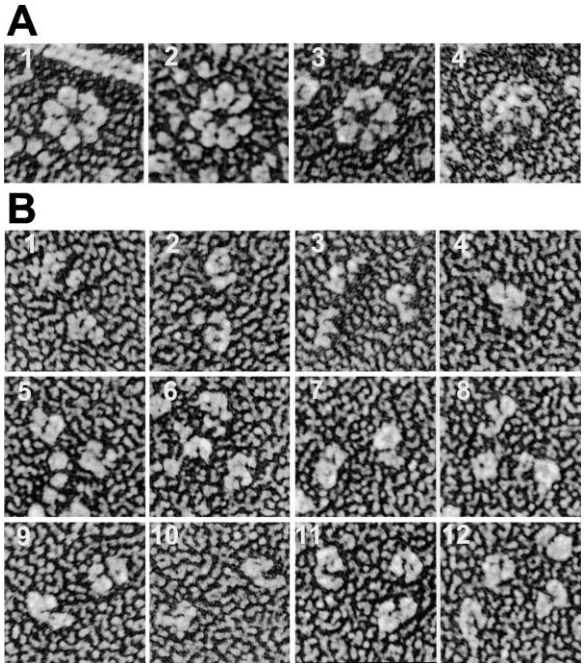

Figure 3. Rotary Shadowing of the Apoptosome and Apaf-1 Monomers

(A) Rotary shadowing confirms the 7-fold symmetry of the apoptosome. Three bottom views and one top view (panel 4) are shown. Actin filaments were added as a control (see panel 1).

(B) A gallery of monomer views is shown for Apaf-1. The monomers appear in distinct conformations, including a Y form (e.g., panels 3, 4, and 8) and a compact form (see panels 5 and 11).

seven- and six-blade β propellers into their respective density. A single cytochrome c was then placed into this region (Figures 4C and 4E) such that its long axis forms a bridge between the β propellers. At higher thresholds, there is a dimple between the two β propellers, and this feature is retained when cytochrome c is docked in this fashion (Figure 4C). It may be possible to place a second cytochrome c at the base of the Y; however, this region may not accommodate the two Apaf-1 linkers and cytochrome c. The small size of cytochrome c would also allow it to be placed in other regions of the spoke. However, cytochrome c would not make contact with the WD40 repeats in these locations. Higher resolution will be required to ascertain whether there are one or two cytochrome c molecules per Apaf-1 in the apoptosome and to identify their orientation(s) (Purring, et al., 1999).

The Apaf-1 CARD represents the active site for procaspase-9 binding. We next placed the Apaf-1 CARD (Qin et al., 1999) within the upper region of the hub domain (Figures 4D and 4E). This assignment produces a good fit and is supported by our identification of the procaspase-9 binding site on the apoptosome (see next section). In addition, we used the constraint that the procaspase-9 CARD should not seriously clash with the apoptosome when the procaspase-9/Apaf-1 CARD-CARD structure is placed within the map.

Based on our analysis, the remaining CED4 homology motif must contribute to the hub domain, the arm, and perhaps to the connection between the lobes of the Y (white dots in Figure 4E). In this model, Apaf-1 is organized in an extended fashion such that the N-terminal region is involved in hub formation, while the C-terminal WD40 repeats form the lobes of the Y domain. Given this molecular topology and the relative volumes of the hub domain and the CARD, it is then possible to estimate the location of the Walker boxes (Walker et al., 1982). These nucleotide binding motifs are probably localized within the lower domain of the hub and the proximal region of the arm. A similar location is deduced for the

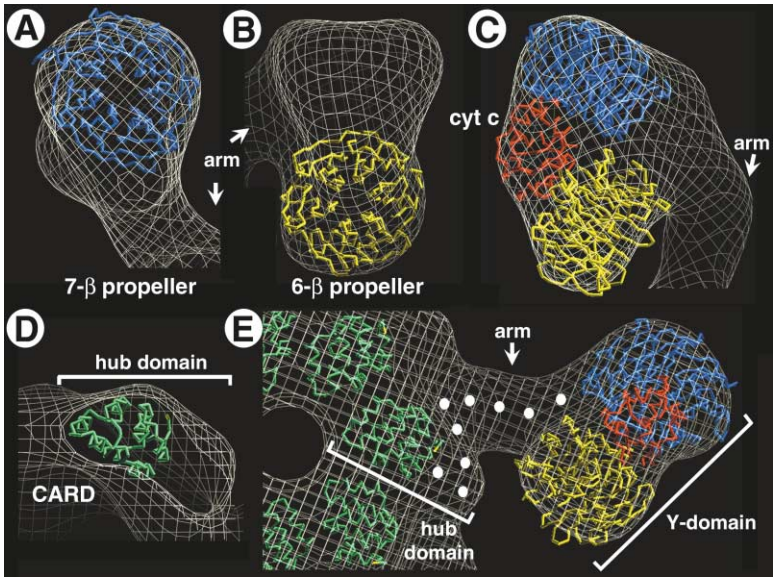

Figure 4. Sequence Motifs and Cytochrome C within the Apoptosome

Representative atomic structures of four domains were positioned within the apoptosome based on their size, shape, and known interactions to identify functional regions.

(A) The seven-bladed β propeller from transducin Gβ was used to model the first seven WD40 repeats in Apaf-1. The larger lobe of the Y domain accommodates the β propeller, as shown by a view along its pseudo 7-fold rotation axis (shown in blue).

(B) The β propeller from TolB was used to model the last six WD40 repeats. The smaller lobe of the Y domain accommodates the six-bladed β propeller, as shown by a view along its pseudo 6-fold rotation axis (shown in yellow).

(C) Cytochrome c (in red; cyt c) was placed in density between the two β propeller domains. A side view of the Y domain is shown with these components. The cytochrome c model was taken from a crystallographic dimer (Takano and Dickerson, 1980).

(D) The Apaf-1 CARD (in green) was placed within the hub at a position adjacent to the central hole. The C-terminal residue is shown in yellow.

(E) The circumferential packing of Apaf-1 CARDs is shown in a top view of the apoptosome. For clarity, only a portion of the hub with one spoke is visible. The three components that were modeled into the Y domain are also included. By subtraction, the intervening regions of the hub and arm must be comprised of the CED4 homology domain (white dots).

Walker boxes, even if Apaf-1 adopts an alternate connectivity within the hub. Thus, nucleotide binding may regulate assembly because the region that contains the Walker boxes may interact directly with the Apaf-1 CARD and also contact the CED4 homology domain in an adjacent monomer (Figure 4E).

The Location of Procaspase-9 on the Apoptosome

Procaspase-9 is comprised of an N-terminal CARD followed by large and small domains. The maturation of procaspase-9 involves a proteolytic cleavage in the loop between the large and small domains to form caspase-9 subunits. This process may require the binding of procaspase-9 molecules in close proximity on the apoptosome, and a D315A mutation creates a poor substrate for cleavage (Srinivasula et al., 1998). We assembled an apoptosome with this procaspase-9 mutant and fractionated the mixture on a Superdex 200 column. Intriguingly, apoptosomes with mutant procaspase-9 are active in cleaving procaspase-3 (Figure 5A, fractions 10 and 11). The fractions were silver stained and revealed a complex of Apaf-1, procaspase-9, and cytochrome c (fraction 10 is shown in Figure 5B). This confirms the observation that procaspase-9 may possess significant proteolytic activity when it associates with the apoptosome (Srinivasula et al., 2001).

Apoptosomes with bound procaspase-9 show a striking tendency to form lateral contacts between particles (data not shown). This microaggregation was not observed in apoptosomes without procaspase-9 and may be due to the zymogen. Edge-on views of apoptosome dimers were also observed at a low frequency in these preparations (Figure 5C). An average map calculated from 22 dimers (see Figure 5C, panel 9) indicates that two apoptosomes are oriented face-to-face within the dimers. Based on the telltale curvature of the edge views (Figure 1E), we deduce that the top surface of each apoptosome is oriented toward the dimer interface. The gap between particles (~100 Å) is too large to allow direct interactions between the hubs. However, material is present between the apoptosomes and appears to link them together (arrowheads in Figure 5C). This material must originate from procaspase-9 bound to the top surface of each apoptosome. Procaspase-9 is tethered to the apoptosome through CARD-CARD interactions with Apaf-1 (Qin et al., 1999). Based on the crystal structures of caspase-9 (Renatus et al., 2001) and its CARD (Qin et al., 1999), we suggest that a procaspase-9 dimer would be the right size to span the gap between apoptosomes.

To identify the binding site for procaspase-9, we determined the 3D structure of an apoptosome with mutant procaspase-9 (Figure 6). Surface views of this map reveal a dome-like feature on the central hub (Figures 6A and 6B). The dome contacts the hub in a region where we had previously modeled the Apaf-1 CARD. However, the dome is too small to contain seven procaspase-9 monomers, which suggests that most of the zymogen is invisible in the 3D map. This may be due to mobility of procaspase-9 on the hub (see Figure 8). Procaspase-9 binding also induces an upward movement of the Apaf-1 CARD (~15 Å) with a concomitant widening of the central hole (Figure 6C). Other details of the spoke are similar in both apoptosomes (compare gold and green maps in Figure 6C).

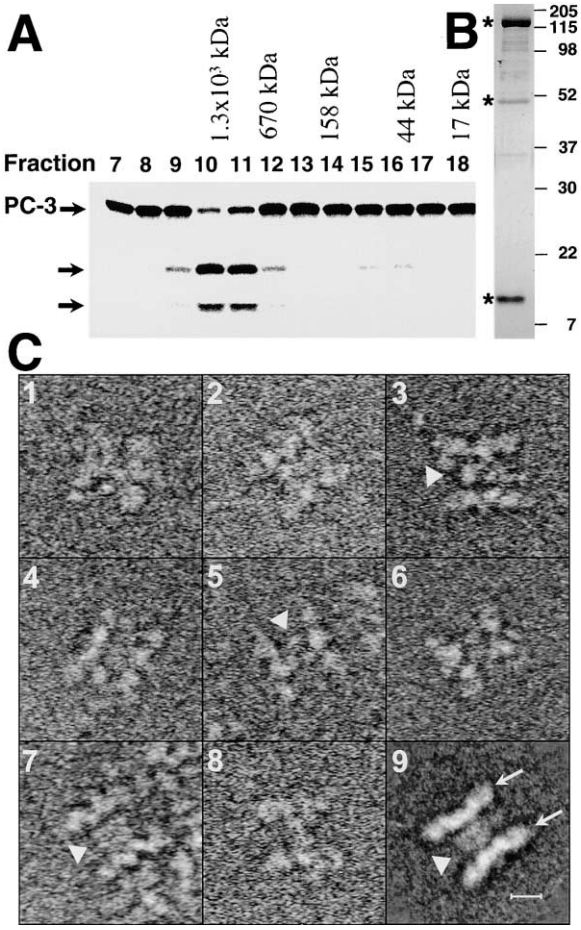

Figure 5. Characteristics of the Apoptosome with Bound Procaspase-9

(A) Apoptosomes with bound procaspase-9 (D315A) were fractionated on a Superdex 200 column, and the fractions were assayed for their ability to activate procaspase-3 by cleaving the zymogen into its two subunits (see arrows). The activity peak coincides with the apoptosome in fractions 10 and 11. Thus, the apoptosome with procaspase-9 (D315A) is a functional activator of procaspase-3.

(B) Fraction 10 was run on an SDS gel and silver stained. The positions of Apaf-1, procaspase-9, and cytochrome c are indicated by stars in descending order, and the positions of the molecular weight markers are shown.

(C) Apoptosomes containing the procaspase-9 mutant are prone to aggregation. In some cases, face-to-face dimers are formed containing two apoptosomes (e.g., panel 9, see white arrows). The dimers have additional material between them, as indicated by the arrowheads in panels 3, 5, 7, and 9. This material may correspond to procaspase-9. The scale bar is 100 Å.

Discussion

Recently, there has been a major effort to provide a structural framework for signaling interactions between death domains and to understand the mechanisms that govern the activation and inhibition of caspases (reviewed by Shi, 2001 and Fesik, 2000). However, there is a paucity of information concerning the structure of Apaf-1 and its interactions with cytochrome c, dATP/ATP, and procaspase-9. In this report, we provide the first structure of the apoptosome and provide a guide to the locations of defined sequence motifs within the

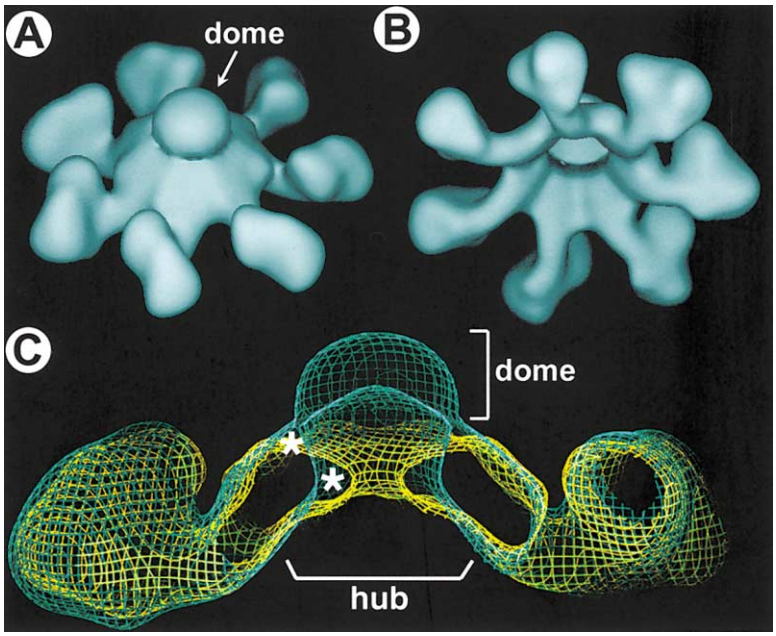

Figure 6. 3D Structure of the Apoptosome with Bound Procaspase-9

(A) An oblique top view is shown of the apoptosome with bound procaspase-9. A central dome-like feature is present on the hub.

(B) A bottom oblique view suggests that the concave surface of the procaspase-9 complex is similar to the apoptosome without procaspase-9.

(C) Density maps for the apoptosome (in yellow) and the procaspase-9 apoptosome (in green) were aligned in "O." A central slab of density suggests that the hub may have an altered conformation when procaspase-9 is bound. This conformational change involves an upward movement of the putative Apaf-1 CARD (see asterisks) and results in a larger diameter for the central pore.

Apaf-1 cytochrome c complex. In a subsequent structure, we identified the procaspase-9 binding site on the apoptosome. When taken together, this work provides a basis for understanding apoptosome assembly and gives insight into the mechanism of procaspase-9 activation.

Apaf-1 within the Apoptosome

In previous work, Apaf-1 was predicted to form a large oligomer in the presence of cytochrome c and dATP/ATP (Zou et al., 1999; Srinivasula et al., 1998). We now show that Apaf-1 and cytochrome c coassemble in vitro to form a wheel-like particle with seven spokes. In addition, the assembly of these complexes is polymorphic, as wheel-like particles with 6-fold symmetry were also observed at a low frequency.

The Apaf-1 molecule has an unusual Y shape that is evident within the apoptosome. Although it is usually difficult to place sequence motifs into a low resolution map, we were able to use biochemical data and crystallographic structures to deduce a self-consistent model for the location of Apaf-1 domains (Figures 7A and 7B). The pattern of 13 WD40 repeats in Apaf-1 suggests that there may be two β propellers comprised of seven and six blades within each spoke. We placed β propellers with different symmetries into the map and found an acceptable solution with seven (transducin Gβ; Gaudet et al., 1996) and six blades (TolB; Carr et al., 1999). We next placed the Apaf-1 CARD within the hub in a position consistent with the location of the procaspase-9 binding site. The remaining CED4 homology motif must be located within the arm, where it may make contributions to the hub and perhaps to the junction between β propellers (Figure 4E). The low resolution of our apoptosome map precluded us from making a pseudo-atomic model by molecular docking. However, the resulting model does allow inferences to be made about assembly and activation.

Our analysis of Apaf-1 suggests that both the CARD and an N-terminal portion of the CED4 homology motif may participate in hub formation. CED4 from *C. elegans* has an N-terminal CARD and oligomerizes but lacks the regulatory WD40 domains (Yang et al., 1998). This suggests that CED4 molecules will form a ring-like oligomer with extended arms but will lack the Y domains. It remains to be seen if other proteins from plants and bacteria with CED4 homology motifs will form rings, as they have different N-terminal adaptors (Aravind et al., 1999).

Assembly of the Apoptosome

Apoptosome assembly is a critical step in the mitochondrial death pathway and requires Apaf-1, cytochrome c, and dATP/ATP (Liu et al., 1996; Goldstein et al., 2000). Apaf-1 is normally inactive and the WD40 repeats may be responsible for maintaining this state, as their deletion results in the constitutive assembly of an active complex (Hu et al., 1998; Srinivasula et al., 1998). A similar defect occurs upon deletion of the WD40 repeats in DARK, a *Drosophila* homolog of Apaf-1 (Rodriguez et al., 1999). The existence of an inactive conformation is also supported by the observation that procaspase-9 CARD will not bind to full-length Apaf-1 in the absence of cytochrome c but readily binds to purified Apaf-1 CARD (Qin et al., 1999). These data suggest that the assembly of a functional apoptosome may require a defined sequence of events. In the first step, cytochrome c binds to Apaf-1 (Liu et al., 1996; Zou et al., 1997; Hu et al., 1999). This is followed by dATP/ATP binding to the CED4 homology domain, which promotes assembly of the apoptosome (Jiang and Wang, 2000). In the final step, procaspase-9 binds to the exposed Apaf-1 CARD to form an active apoptosome.

We now propose an assembly model for the apoptosome that incorporates known biochemical and structural data. Our studies suggest that cytochrome c may bind between the two WD40 β propellers. We also note that the Apaf-1 CARD and the region of the CED4 homol-

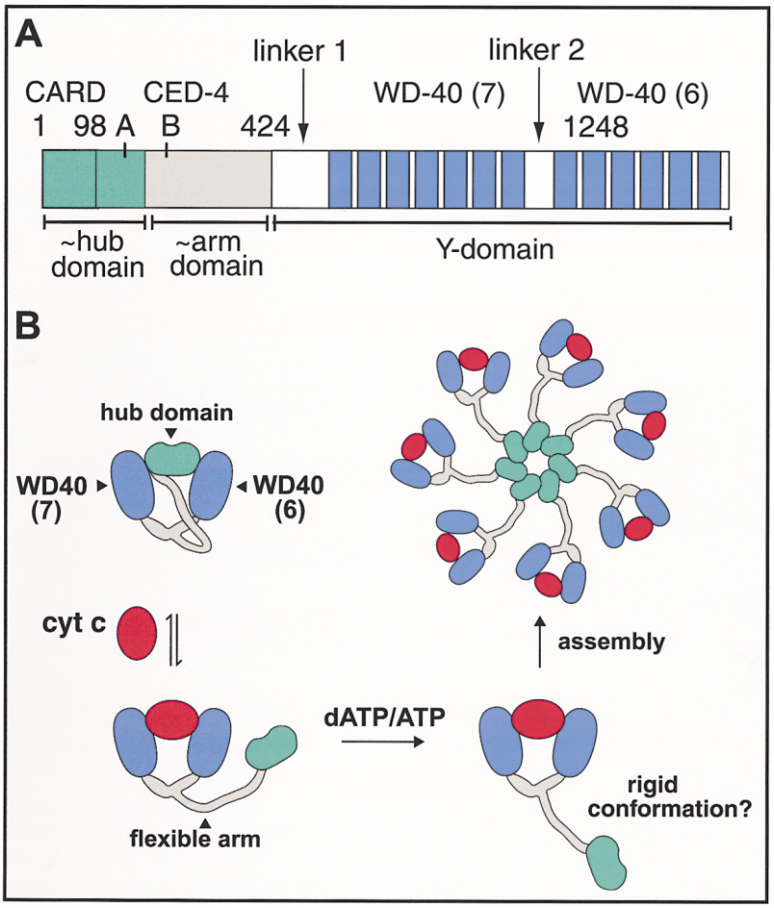

Figure 7. The Role of Apaf-1 Sequence Motifs in the Assembly of an Apoptosome

(A) The relative positions of the CARD, CED4 homology motif, WD40 repeats, and linker regions are shown on a linear map of Apaf-1. The approximate positions of the hub, the arm, and the Y domains are indicated and color-coded. The positions of the Walker A and B nucleotide binding motifs are shown. Thus, the nucleotide binding pocket may be located in close proximity to the hub, where it may regulate assembly.

(B) Apaf-1 normally adopts an autoinhibited conformation in healthy cells (top left). In actuality, only one globular region of the hub domain may interact directly with the β propellers. Cytochrome c then displaces the hub domain (left side), which allows Apaf-1 to bind dATP/ATP (bottom). Upon nucleotide binding, a second conformational change may promote assembly (right side). For clarity, the length of the arm has been extended in this diagram.

ogy motif within the hub domain are each similar in size to cytochrome c. Indeed, computer modeling indicates that the Apaf-1 CARD will fit between the β propellers. Therefore, we propose that one or both of the globular regions within the hub domain may bind between the two β propellers to generate an autoinhibited conformation (Figure 7B, top left). This autoinhibited Apaf-1 would have a compact shape, similar to particles observed in rotary shadowing experiments (Figure 3B). The formation of a compact monomer would also require the CED4 homology domain to be intrinsically flexible. As apoptosome assembly is a tightly regulated process, it is unlikely that the extended Y conformation of Apaf-1 (Figure 3B) would coexist with the compact monomer in the absence of cytochrome c. Perhaps interactions with the mica surface are responsible for a limited "unfolding" of the compact monomer to form the Y-shaped molecules observed in our experiment.

We suggest that cytochrome c may displace one hub domain from between the β propellers (Figure 7B, bottom left). This in turn would allow the CED4 homology domain to bind dATP/ATP and undergo a conformational change. Two conditions may be required for efficient assembly. First, cytochrome c must be present so that the hub domains are free to assemble into the hub. Second, nucleotide binding may lock the CED4 homology domain into a more extended conformation that would prevent the hub domain from reassociating with the β propellers (Figure 7B, right side). In this model, the Apaf-1 arm must have at least one flexible joint that becomes more rigid upon binding dATP/ATP. The Walker A and B boxes participate in nucleotide binding and are centered on Apaf-1 residues 145 and 230 (Zou et al., 1997; Walker et al., 1982). Our model for the topology of Apaf-1 suggests that the nucleotide binding site may be located within the hub and the proximal region of the arm. Thus, conformational changes associated with dATP/ATP binding could be transmitted to both the hub domain and the arm.

Cytochrome c has been chosen during evolution to promote assembly of Apaf-1 into the apoptosome. A primary consideration in this selection may have been that holo-cytochrome c is never found in the cytosol but instead is sequestered within mitochondria. The choice of cytochrome c may also have depended upon the fact that it is similar in size to the Apaf-1 CARD and the globular region of CED4 within the hub domain. Hence, it is well suited to regulate assembly by a mechanism of physical displacement. This model also explains why cytochrome c binding to the β propellers may enhance the nucleotide affinity of the CED4 homology domain (Jiang and Wang, 2000). Release of the hub domain from the chaperone-like environment of the β propellers would allow the CED4 homology domain to adopt conformations with a higher nucleotide affinity. The model also explains the observed synergism between procaspase-9 and nucleotide binding (Jiang and Wang, 2000). In the presence of cytochrome c, an equilibrium may

exist between Apaf-1 molecules that have bound their own hub domain and those which have bound cytochrome c (Figure 7B, left side). If procaspase-9 is present, then it would bind to the exposed Apaf-1 CARD and likely prevent the hub domain from reassociating with the β propellers. Therefore, procaspase-9 should enhance nucleotide binding to Apaf-1 and promote assembly of the apoptosome.

Overall, this model suggests that Apaf-1 sequence motifs have functions that are distinct yet complementary. The Apaf-1 CARD has at least three functions. First, it may be bound between the two WD40 β propellers to render Apaf-1 inactive. Second, it plays a critical role in forming the central hub of the apoptosome. Third, the CARD provides a binding site for procaspase-9. The CED4 homology motif also has multiple functions. It forms the lower domain within the hub, and in concert with the proximal region of the arm, binds dATP/ATP to promote assembly. In addition, the CED4 homology motif forms the arm, which may be a key element in regulating assembly by virtue of its flexibility. Finally, the role for two WD40 domains is now apparent; by acting together the β propellers may jointly sequester the hub domain to inhibit assembly. Thus, cytochrome c may be an efficient activator because it is able to displace the hub domain from between the β propellers.

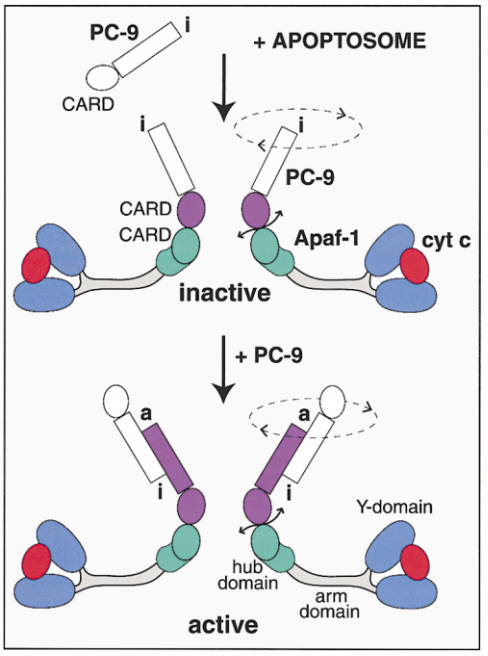

Figure 8. A Model for Procaspase-9 Activation on the Apoptosome

In solution, procaspase-9 is a monomer with an inactive catalytic site (marked with an "i"). In the first step of activation, procaspase-9 binds to the central hub of the apoptosome through CARD-CARD interactions. At this point, the bound procaspase-9 monomer is mobile (indicated by circular arrows) and inactive. A second procaspase-9 molecule from solution may then associate with bound procaspase-9 to form a dimer containing one active catalytic site (marked with an "a") and one inactive site (Renatus et al., 2001). We suggest that the active catalytic site for each caspase-9 dimer would be formed by the monomer that is bound to the apoptosome by its CARD. Proteolytic cleavage then generates the mature caspase-9 dimer.

The Activation of Procaspase-9

The atomic structures of caspase-1, -3, -7, -8, and -9 are known (see Fesik, 2000; Renatus et al., 2001). In all cases, the active enzyme is a dimer formed by monomers packed in an antiparallel manner. In turn, each monomer is comprised of large and small subunits, derived by proteolysis of the loop between corresponding domains of the zymogen (Kumar and Colussi, 1999). Recent data indicate that caspase-9 without a CARD is a monomer in solution (Renatus et al., 2001). However, caspase-9 will form dimers in the presence of a peptide inhibitor or at the high concentrations required for crystallization. In addition, proteolytic assays suggest that the dimer possesses significant activity while the monomer is inactive. Remarkably, a crystal structure of the caspase-9 dimer without CARDs suggests that only one catalytic site has an active conformation, as reflected by a covalently bound peptide inhibitor. The second site remains inactive due to an altered positioning of the activation loop (Renatus et al., 2001). This asymmetry does not arise from crystal contacts and may be an intrinsic property of the caspase-9 dimer.

The structure of a dimeric procaspase-7 highlights the important role of the interdomain loop in activation (Chai et al., 2001). Proteolytic cleavage of this loop promotes the formation of an active catalytic site within each caspase-7 monomer. However, procaspase-9 is unusual because it exhibits a low but significant level of processing activity (~10%; Stennicke et al., 1999). Intriguingly, the interdomain loop is longer in procaspase-9, and this feature may allow the zymogen to adopt an active conformation. In our work, a cleavage site mutant of procaspase-9 (D315A) showed significant proteolytic activity when bound to the apoptosome (Figure 5A). Thus, procaspase-9 activation may require the zymogen to bind to the apoptosome as a monomer where it may subsequently form active dimers. This in turn suggests that proteolytic cleavage may be more important in downregulating procaspase-9 on the apoptosome, as IAPs bind to the exposed N terminus of the caspase small subunit (Srinivasula et al., 2001; Shi, 2001).

We next showed that procaspase-9 binds to the central hub of the apoptosome at a site consistent with the Apaf-1 CARD position deduced by modeling. Unexpectedly, we found that a large part of the procaspase-9 molecule is invisible in the map. This is presumably due to a flexible link between the procaspase-9 CARD and the large domain. In addition, procaspase-9 binding to the apoptosome may induce the Apaf-1 CARD to undergo a conformational change and become more mobile. Given that procaspase-9 is tethered to the apoptosome in a flexible manner, why is it incapable of undergoing proteolytic activation in solution? Perhaps the free CARD of procaspase-9 may downregulate zymogen activity by interfering with dimer formation. In support of this model, caspase-9 has much greater activity when bound to the apoptosome than when free in solution (Rodriguez and Lazebnik, 1999; Stennicke et al., 1999).

We now present a model for procaspase-9 activation on the apoptosome. The stoichiometry of Apaf-1 CARD to procaspase-9 CARD is one-to-one (Zou et al., 1999; Qin et al., 1999), and the apoptosome has 7-fold symme-

try. Hence, seven procaspase-9 molecules are required to saturate binding sites on the apoptosome. At this stage, the catalytic sites of procaspase-9 monomers would extend into solution but remain inactive (Figure 8, top). The high local concentration of procaspase-9 on the hub may then facilitate the recruitment of monomers from solution to form dimers. Importantly, each of the procaspase-9 dimers would contain a single active catalytic site (Figure 8, bottom; Renatus et al., 2001). As procaspase-9 in solution is inactive, we suggest that the monomer with a free CARD would be inactive. This model also places the active catalytic sites distal to the hub surface where there is less steric hindrance for substrate binding. Proteolysis of the interdomain loop would then generate mature caspase-9. We suggest that the subsequent cleavage of procaspase-3 may utilize the flexibility of the bound caspase-9 molecules. This property of caspase-9 may promote the binding of multiple procaspase-3 zymogens to the apoptosome and enhance the efficiency of activation.

This model also reconciles the apparent symmetry mismatch between Apaf-1 and the procaspase-9 dimer. The activation of procaspase-9 generates a strict one-to-one correspondence between active catalytic sites and Apaf-1 monomers within the apoptosome. Given that procaspase-9 and caspase-9 may both be dimers on the apoptosome, it is then possible to form a larger complex in which two apoptosomes are linked together. Further experiments are now required to ascertain the oligomeric state of caspase-9 on the apoptosome and to evaluate the possible significance of the apoptosome dimer.

Experimental Procedures

Apaf-1 Complexes and the Activation Assay

A His-tagged isoform of Apaf-1 (Apaf-1-1L-WD13) and a D315A mutant of procaspase-9 were overexpressed and purified (Zou et al., 1999; Jiang and Wang, 2000). For the purification of procaspase-9, a further heparin chromatography was performed. A 1 ml HiTrap heparin column (Amersham Pharmacia Biotech) was used, and procaspase-9 was eluted with 0–200 mM NaCl gradient in buffer A (20 mM HEPES-KOH [pH 7.5], 10 mM KCl, 1.5 mM $MgCl_2$, 1 mM EDTA, 1 mM EGTA, 1 mM dithiothreitol, and 1 mM phenylmethylsulfonyl fluoride). Horse cytochrome c was obtained as described (Liu et al., 1996), and dATP was purchased from Amersham Pharmacia Biotech. Frozen aliquots were used immediately upon thawing to set up assembly reactions at 30°C for periods of 30–60 min. Apaf-1 in buffer A (Jiang and Wang, 2000) at ~0.4 mg/ml was mixed with cytochrome c in a range of molar ratios from 1:1 to 1:2, and dATP was added to a final concentration of 0.1 mM. For experiments with procaspase-9, buffer A was supplemented with 5 mM $MgCl_2$ and 25 mM NaCl, and the procaspase-9/Apaf-1 molar ratio was 1.2:1. After assembly was complete, Nonidet P40 was added to the samples prior to freezing to give a final concentration of 0.01%.

Procaspase-3 processing activity was assayed as follows. In a 60 μl incubation, 0.1 mg/ml BSA, 1.5 μM Apaf-1, 5 μM cytochrome c, 1 mM dATP, and 3 μM D315A procaspase-9 were mixed with buffer A containing 5 mM $MgCl_2$ and incubated at 30°C for 1 hr. Subsequently, 50 μl of the mixture was fractionated on a Superdex 200 column in a Smart chromatography system (Amersham Pharmacia Biotech). The column was eluted with buffer C (20 mM HEPES-KOH [pH 7.5], 10 mM KCl, 50 mM NaCl, 5 mM $MgCl_2$, and 1 mM dithiothreitol). Procaspase-3 cleavage activity of the fractions was measured by incubating 20 μl of each fraction with 1 μl of ^{35}S-methione-labeled procaspase-3 at 30°C for 1 hr followed by SDS-PAGE, protein transfer to a nitrocellulose membrane, and phosphorimaging as described previously (Liu el al., 1996).

Electron Cryomicroscopy and Image Processing

Two microliter aliquots of assembled complexes were pipetted onto hydrophobic holey carbon films on 400 mesh Cu grids. Holey grids were also obtained from Quantifoil and used after stabilization with additional carbon. Specimens were blotted and plunged into liquid ethane at a relative humidity of at least 85% at 4°C. A Gatan cryotransfer system and cryoholder (626-DH) were used to transfer grids into a CM12 electron microscope equipped with a cryo-blade-type anticontaminator, a specimen relocation system, and a LaB6 filament. Electron micrographs were recorded at 35,000× magnification on KODAK SO163 with minimal dose at 100 kV.

Micrographs were evaluated by optical diffraction, and those with minimal astigmatism and drift were processed. Negatives were digitized with a Zeiss SCAI scanner with a 7 μm step size, subsequently binned to a pixel size of 14 μm (corresponding to 4 Å/pixel), and converted to MRC format. Particles were selected from the images in the EMTOOL package. The 3D image processing was carried out with EMAN (Ludtke et al., 1999) and SPIDER (Frank et al., 1996). In all, ~3400 particles with a nominal defocus range of –1.5 to –3.5 μm were used in three major defocus groups. An initial 3D model for the apoptosome was obtained from the most strongly defocused images using EMAN. Top and side views were merged to form the first 3D model using the C7 rotational symmetry of the particle. This model was refined within EMAN using cycles of classification and projection matching to assign Euler angles. This model was then used to refine two additional datasets with lower defocus to provide intermediate 3D structures. The CTF parameters were determined for individual micrographs, and the corresponding particles corrected for the CTF phase flips in SPIDER. The combined data were then refined in EMAN to produce a final 3D map of the apoptosome with good angular sampling. The final 3D model retained all major features of the intermediate structures. The resolution was estimated with the Fourier shell correlation using a cutoff of 0.5.

The structure of the apoptosome with bound procaspase-9 was determined using a noncleavable mutant (D315A). In this work, ~5400 particles with a defocus of about –2.5 μm were CTF corrected and processed to provide the final 3D structure. The lowest resolution 3D model of the apoptosome was used as the first reference (Figure 1A). A larger number of particles were used to provide accurate class averages within the asymmetric triangle because the particles tended to orient preferentially within the ice. Edge-on views of apoptosome dimers (~22) were aligned in SPIDER to provide an average. Images of Apaf-1 monomers and apoptosomes were obtained by rotary shadowing using the technique of Heuser (1989). Graphics were prepared using WEB (Frank et al., 1996) and "O" (Jones et al., 1991). Models of β propellers with seven blades (transducin Gβ/1GFW; Gaudet et al., 1996) and six blades (TolB/1CRZ; Carr et al., 1999) were manually positioned within the 3D map of the apoptosome based on their size and shape. A similar process was carried out with cytochrome c (3CYT; Takano and Dickerson, 1980) and the Apaf-1 CARD (3YGS; Qin et al., 1999).

Acknowledgments

We thank H. Zou for initial samples of the apoptosome, T. Rapoport for providing the Zeiss scanning densitometer, J. Head and D. Thomas for helpful comments on "O," and Y. Li and F. Du for preparing recombinant proteins. We are indebted to S. Ludtke for providing the EMAN software package. Both the C.W.A. and X.W. laboratories are supported by NIH grants, and X.W. is also supported by the Welch Foundation.

Received September 6, 2001; revised October 18, 2001.

References

Aravind, L., Dixit, V.M., and Koonin, E.V. (1999). The domains of death: evolution of the apoptosis machinery. Trends Biochem. Sci. *24*, 47–52.

Budihardjo, I., Oliver, H., Lutter, M., Luo, X., and Wang, X. (1999). Biochemical pathways of caspase activation during apoptosis. Annu. Rev. Cell Dev. Biol. *15*, 269–290.

Carr, S., Penfold, C.N., Bamford, V., James, R., and Hemmings, A.M.

(1999). The structure of TolB, an essential component of the tol-dependent translocation system, and its protein-protein interaction with the translocation domain of colicin E9. Structure *8*, 57–66.

Chai, J., Wu, Q., Shiozaki, E., Srinivasula, S.M., Alnemri, E.S., and Shi, Y. (2001). Crystal structure of a procaspase-7 zymogen: mechanisms of activation and substrate binding. Cell *107*, 399–407.

Desagher, S., and Martinou, J.-C. (2000). Mitochondria as the central control point of apoptosis. Trends Cell Biol. *10*, 369–377.

Fesik, S.W. (2000). Insights into programmed cell death through structural biology. Cell *103*, 273–282.

Frank, J., Radermacher, M., Penczek, P., Ladjadj, M., and Leith, A. (1996). SPIDER and WEB: processing and visualization of images in 3D electron microscopy and related fields. J. Struct. Biol. *116*, 190–199.

Gaudet, R., Bohm, A., and Sigler, P.B. (1996). Crystal structure at 2.4 Å resolution of the complex of transducin Gβ and its regulator, phosducin. Cell *87*, 577–588.

Goldstein, J.C., Waterhouse, N.J., Juin, P., Evan, G.I., and Green, D.R. (2000). The coordinate release of cytochrome c during apoptosis is rapid, complete and kinetically invariant. Nat. Cell Biol. *2*, 156–162.

Heuser, J. (1989). Procedure for 3-D visualization of molecules on mica via the quick-freeze, deep-etch technique. J. Electron Micros. Technique *13*, 244–263.

Hu, Y., Ding, L., Spencer, D.M., and Nunez, G. (1998). WD-40 repeat region regulates Apaf-1 self-association and procaspase-9 activation. J. Biol. Chem. *273*, 33489–33494.

Hu, Y., Benedict, M.A., Ding, L., and Nunez, G. (1999). Role of cytochrome c and dATP/ATP hydrolysis in Apaf-1 mediated caspase-9 activation and apoptosis. EMBO J. *18*, 3586–3595.

Jiang, X., and Wang, X. (2000). Cytochrome c promotes caspase-9 activation by inducing nucleotide binding to Apaf-1. J. Biol. Chem. *275*, 31199–31203.

Jones, T.A., Zou, J.-Y., and Cowan, S.W. (1991). Improved methods for building protein models in electron density maps and the location of errors in these models. Acta Crystallogr. A *47*, 110–119.

Kumar, S., and Colussi, P.A. (1999). Prodomains, adaptors, oligomerization: the pursuit of caspase activation in apoptosis. Trends Biochem. Sci. *24*, 1–4.

Li, P., Nijhawan, D., Budihardjo, I., Srinivasula, S.M., Ahmad, M., Alnemri, E.S., and Wang, X. (1997). Cytochrome c and dATP-dependent formation of Apaf-1/caspase-9 complex initiates an apoptotic protease cascade. Cell *91*, 479–489.

Li, K., Li, Y., Shelton, J.M., Richardson, J.A., Spencer, E., Chen, Z.J., Wang, X., and Williams, R.S. (2000). Cytochrome c deficiency causes embryonic lethality and attenuates stress-induced apoptosis. Cell *101*, 389–399.

Liu, X., Kim, C.N., Yang, J., Jemmerson, R., and Wang, X. (1996). Induction of apoptotic program in cell free extracts: requirement for dATP and cytochrome c. Cell *86*, 147–157.

Ludtke, S.J., Baldwin, P.R., and Chiu, W. (1999). EMAN: semiautomated software for high-resolution single-particle reconstructions. J. Struct. Biol. *128*, 82–97.

Purring, C., Zou, H., Wang, X., and McLendon, G. (1999). Stoichiometry, free energy and kinetic aspects of cytochrome c: Apaf-1 binding in apoptosis. J. Am. Chem. Soc. *121*, 7435–7436.

Qin, H., Srinivasula, S.M., Wu, G., Fernandes-Alnemri, T., Alnemri, E.S., and Shi, Y. (1999). Structural basis of procaspase-9 recruitment by the apoptotic protease-activating factor 1. Nature *399*, 549–557.

Renatus, M., Stennicke, H.R., Scott, F.L., Liddington, R.C., and Salvesen, G.S. (2001). Dimer formation drives the activation of the cell death protease caspase-9. Proc. Natl. Acad. Sci. USA *98*, 14250–14255.

Rodriguez, J., and Lazebnik, Y. (1999). Caspase-9 and Apaf-1 form an active holoenzyme. Genes Dev. *13*, 3179–3184.

Rodriguez, A., Oliver, H., Zou, H., Chen, P., Wang, X., and Abrams, J.M. (1999). Dark is a *Drosophila* homologue of Apaf-1/CED4 and functions in an evolutionarily conserved death pathway. Nat. Cell Biol. *1*, 272–275.

Salvesen, G.S., and Dixit, V.M. (1997). Caspases: intracellular signaling by proteolysis. Cell *91*, 443–446.

Shi, Y. (2001). A structural view of mitochondria-mediated apoptosis. Nat. Struct. Biol. *8*, 394–401.

Smith, T.F., Gaitatzes, C., Saxena, K., and Neer, E.J. (1999). The WD repeat: a common architecture for diverse functions. Trends Biochem. Sci. *24*, 181–184.

Song, Z., and Steller, H. (1999). Death by design: mechanism and control of apoptosis. Trends Cell Biol. *12*, 49–52.

Srinivasula, S.M., Ahmad, M., Fernandes-Alnemri, T., and Alnemri, E.S. (1998). Autoactivation of procaspase-9 by Apaf-1 mediated oligomerization. Mol. Cell *1*, 949–957.

Srinivasula, S.M., Hegde, R., Saleh, A., Datta, P., Shlozakl, E., Chal, J., Lee, R., Robbins, P.D., Fernandes-Alnemri, T., Shi, Y., and Alnemri, E.S. (2001). A conserved XIAP-interaction motif in caspase-9 and Smac/DIABLO regulates caspase activity and apoptosis. Nature *410*, 112–116.

Stennicke, H.R., Deveraux, Q.L., Humke, E.W., Reed, J.C., Dixit, V.M., and Salvesen, G.S. (1999). Caspase-9 can be activated without proteolytic processing. J. Biol. Chem. *274*, 8359–8362.

Takano, T., and Dickerson, R.E. (1980). Redox conformation in refined tuna cytochrome c. Proc. Natl. Acad. Sci. USA *77*, 6371–6375.

Thompson, C.B. (1995). Apoptosis in the pathogenesis and treatment of disease. Science *267*, 1456–1462.

Walker, J.E., Saraste, M., Runswick, M.J., and Gay, N.J. (1982). Distantly related sequences in the alpha- and beta-subunits of ATP synthase, myosin, kinases and other ATP-requiring enzymes and a common nucleotide binding fold. EMBO J. *1*, 945–951.

Yang, X., Chang, H.Y., and Baltimore, D. (1998). Essential role of CED4 oligomerization in CED-3 activation and apoptosis. Science *281*, 1355–1357.

Zou, H., Henzel, W.J., Liu, X., Lutschg, A., and Wang, X. (1997). Apaf-1, a human protein homologous to *C. elegans* CED4, participates in cytochrome c dependent activation of caspase-3. Cell *90*, 405–413.

Zou, H., Li, Y., Liu, X., and Wang, X. (1999). An Apaf-1 cytochrome c multimeric complex is a functional apoptosome that activates Procaspase-9. J. Biol. Chem. *274*, 11549–11556.